*J. Chem. Sci.* (2020)132:54
https://doi.org/10.1007/s12039-020-1758-7


REGULAR ARTICLE

# Photoelectrochemical detection of chromium (VI) using layered $MoS_2$ modified BiOI

RU CHEN[a,*], RONGQING TANG[b] and CHENG CHEN[a]
[a]Kaifeng Quality and Technical Supervision, Inspection and Testing Center, Kaifeng 475000, China
[b]Mining Technology College, Liaoning University of Engineering and Technology, Jinzhou 125105, Liaoning, China
E-mail: chensiru@126.com

MS received 25 July 2019; revised 17 November 2019; accepted 24 November 2019

**Abstract.** In recent years, BiOI has been extensively studied due to its excellent absorption ability of visible light. However, low energy conversion efficiency affects its potential for practical application. In this paper, $MoS_2$/BiOI composite was synthesized by two-step ways and applied to the photoelectrochemical (PEC) detection of hexavalent chromium (Cr (VI)). Through a series of optical characterization, the structure and morphology of the material were measured in detail. UV–Vis diffuse reflection spectra and photoluminescence (PL) further proved that $MoS_2$/BiOI have the excellent PEC properties. The PEC experiment proved that the prepared $MoS_2$/BiOI has a wide linear range (0.05–160 μM) and low detection limit (0.01 μM, at S/N = 3), moreover, it has great application potential in actual samples.

**Keywords.** Energy conversion; $MoS_2$/BiOI; Photoelectrochemical; Detection; Chromium.

## 1. Introduction

In the past few decades, the amount and complexity of pollutants discharged into global water bodies have increased.[1] Therefore, the search for environmentally friendly wastewater management methods has attracted people's attention. Hexavalent chromium (Cr (VI)) has attracted the attention of many researchers because of its high toxicity, carcinogenic and mutagenicity actions for human health.[2,3] Furthermore, most reports showed that chromium has caused environmental hazards.[4,5] Therefore, a reliable and rapid chromium detection technology is urgently needed.

Up to now, photoelectrochemical (PEC) detection, as a reliable and fast-developing technology, has been fruitfully used to the resolve of Cr (VI) in water due to its good selectivity, low cost, wide applicability and low background signal.[6,7] In the PEC process, photoelectrochemistry has optical and electrical advantages during PEC testing, which has aroused the interest of researchers.[8,9] With the rapid development of PEC technology, a large number of materials with PEC properties have emerged, such as oxide-, sulfide- and Bi-based photocatalysts.[10–12] Among them, bismuth-system based oxides consist of 6s Bi orbital Bi orbitals and 2p oxygen orbitals, which showed high photocatalytic activity and good electrical properties.[13,14] BiOX (X = Cl, I, Br) have attracted extensive attention in the field of PEC due to its abundance, low toxicity and low cost.[15–17]

Much attention has been given to BiOI, a p-type semiconductor with great visible light absorption capacity because of its small bandgap (1.8 eV).[18] Moreover, the unique layered structure of BiOI is conducive to excellent photocatalytic activity.[19,20] However, BiOI owns a narrow bandgap semiconductor, which leads to swift recombination of photogenerated electrons and holes.[21] Therefore, in order to enhance PEC properties of BiOI, the heterostructure is formed by coupling BiOI using other semiconductor materials, such as $BiPO_4$/BiOI,[22] $TiO_2$/BiOI,[23] $BiVO_4$/BiOI.[24]

$MoS_2$ has good photocatalytic performance due to the special structure of S-Mo-S atoms sandwich layers.[25,26] Furthermore, recent research indicated that $MoS_2$ displayed superior photocatalytic activity, because of its unique electrical and optical properties, large surface area.[27] Thus, $MoS_2$ has been used to couple several materials, including $BiVO_4$,[28] $WS_2$,[29] $TiO_2$,[30] which can promote electron-hole pair separation and enhance PEC performance.

*For correspondence

Published online: 13 March 2020

In this work, the material of $MoS_2$/BiOI were successfully synthesized by two-step ways, and PEC sensor of the Cr (VI) using $MoS_2$/BiOI on ITO glass as the electrode was reported. The PEC experiments show that $MoS_2$/BiOI-5 has excellent PEC performance compared to pure $MoS_2$ and BiOI, and it exhibits wide linear range (0.05–160 μM), low detection limit (0.01 μM, at S/N = 3) and excellent selectivity for detecting Cr (VI). The results show that the sensor based on $MoS_2$/BiOI-5 has a good application prospect in the detection of Cr (VI).

## 2. Experimental

### 2.1 *Reagents*

All reagents are analytical and can be applied without further purification. $Bi(NO_3)_3{\cdot}5H_2O$, $(NH_4)_6Mo_{24}{\cdot}4H_2O$ and $SC(NH_2)_2$, KI, ethanol, ethylene glycol (EG) and acetone were sourced from Sinopharm Chemical Reagent Co., Ltd (www.sinoreagent.com).

### 2.2 *Preparation of the $MoS_2$/BiOI heterojunction*

The composite materials were prepared in two steps. Firstly, $MoS_2$ was synthesized. $(NH_4)_6Mo_{24}{\cdot}4H_2O$ and $SC(NH_2)_2$ were dissolved in deionized water under stirring. Then, these were transferred to a 100 mL Teflon-lined stainless steel autoclave, and heated at 200 °C for 24 h. The obtained product was $MoS_2$. Secondly, the $MoS_2$/BiOI heterojunction was prepared. An appropriate amount of KI was dissolved in the mixed solution of EG and $H_2O$. Then, an appropriate amount of $Bi(NO_3)_3{\cdot}5H_2O$ and the synthesized $MoS_2$ were slowly added to the suspension obtained above and continuously stirred for half an hour. The mixed solution was heated at 180 °C for 24 h in 100 mL Teflon-lined autoclave. Finally, the product was continually washed three times together with deionized water and ethanol and then dried at 60 °C for 12 h. It is essential to mention that $MoS_2$ added to the mass fraction of 5% was recorded as $MoS_2$/BiOI-5. According to a similar method, dissimilar $MoS_2$/BiOI-2 and $MoS_2$/BiOI-7 (2 wt% and 7 wt%) were manufactured individually.

### 2.3 *Characterization*

On a Bruker D8 Advance diffractometer with Cu Kα radiation x-ray diffraction patterns were done successfully. The X-ray photoelectron spectrum was obtained by X-ray photoelectron spectroscope. Diffuse reflection spectra (DRS) of the examples were taken on a UV–Vis spectrophotometer with $BaSO_4$ as reference. The morphology of the samples was characterized by scanning electron microscopy (SEM) and transmission electron microscope. The photoluminescence spectrum was characterized by 370 nm excitation wavelength.

### 2.4 *Electrochemical experiments*

All electrochemical experiments were carried out on a CHI 660E electrochemical workstation, which has a three-electrode system, and used Pt wire and saturated calomel electrode (SCE) as counter electrode and reference electrode correspondingly. The working electrode is indium tin oxide (ITO) glass deposited from synthetic composite materials. Xenon lamps, with the condition of PLS-SXE 300, 100 mW $cm^{-2}$, $\lambda \geq 420$ nm, were used as light sources. Electrochemical impedance spectroscopy is performed from frequency (Hz) 1–1,000,000. Indium tin oxide electrode was washed with water, acetone and ethanol for 5 min, respectively. Then 3 mg of catalyst powder was dispersed in 1 mL of deionized water and 300 μL chitosan to form a uniform suspension. Then, 20 μL suspensions were coated on ITO electrode (0.5 $cm^2$).

## 3. Results and Discussions

### 3.1 *Choice of materials*

The phases of all prepared materials were studied by XRD (Figure 1). For pure BiOI (Figure 1a), the four obvious characteristic peaks around 29.64°, 31.66°, 45.67° and 55.15° correspond to (102), (110), (104) and (212) of BiOI (JCPDS 10-0445). While the peaks at 12.6°, 31.2°, 34.6° (Figure 1e) were attributed to the (002), (100), (102) lattice plane of $MoS_2$ (JCPDS No. 37-1492). For $MoS_2$/BiOI, the positions of the peaks are the same for different composites, with both BiOI and $MoS_2$ peaks clearly identifiable. Furthermore, with the increase of $MoS_2$, the peak of (002) became more

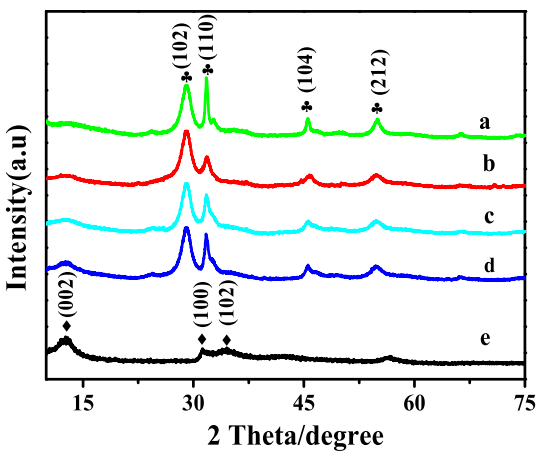


**Figure 1.** XRD profile of $MoS_2$ (e), BiOI (a), $MoS_2$/BiOI-2 (b), $MoS_2$/BiOI-5 (c) and $MoS_2$/BiOI-7 (d) composites.

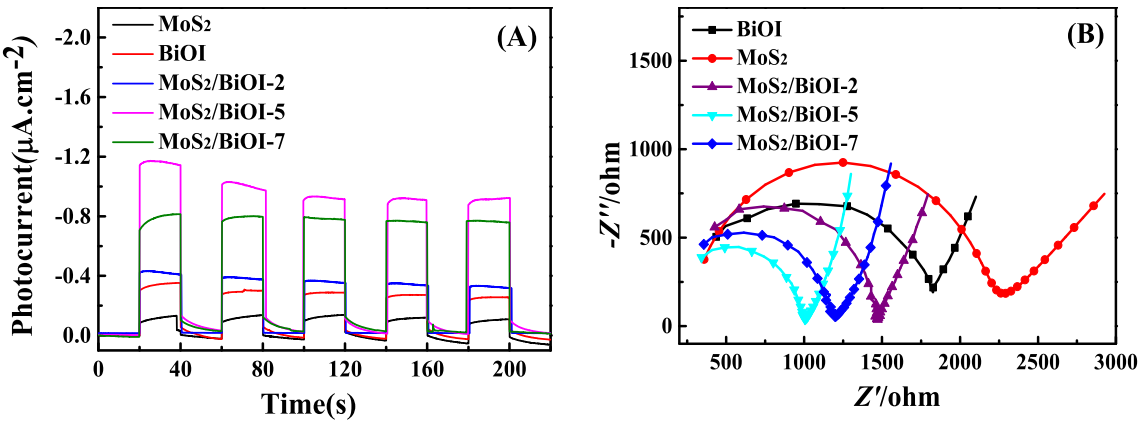


**Figure 2.** Photocurrent responses (a), and EIS (b) of the $MoS_2$, BiOI and $MoS_2$/BiOI composites in 0.1 M PBS.

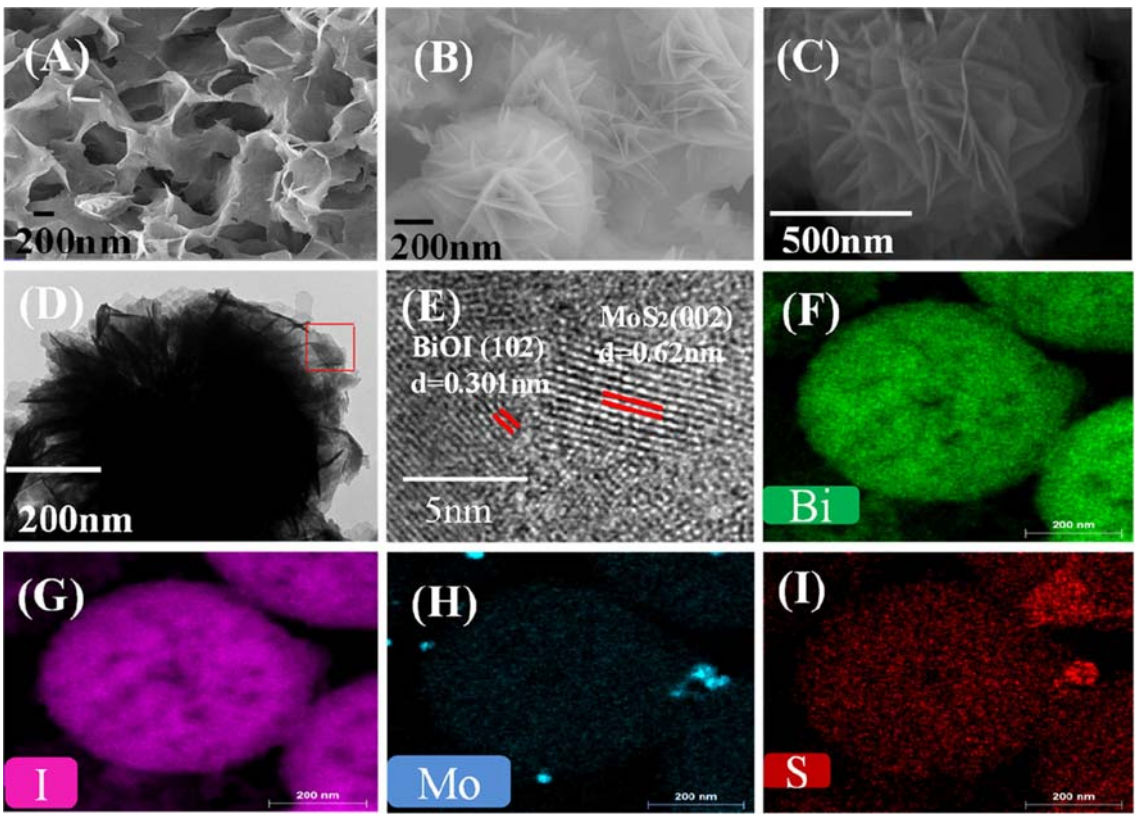


**Figure 3.** FESEM images of $MoS_2$ (a), BiOI (b), SEM (c), TEM (d) and HRTEM (e) images of $MoS_2$/BiOI-5; Mapping images (f) Bi (g) I (h) Mo (i) S of $MoS_2$/BiOI-5.

and more obvious. All results show that we have successfully synthesized $MoS_2$/BiOI.

In order to further evaluate PEC performance $MoS_2$, BiOI and $MoS_2$/BiOI-X, Figure 2a shows photocurrent densities of all materials under visible light irradiation in 0.1 M PBS. The photocurrent densities of all materials can be as: $MoS_2$/BiOI-5 > $MoS_2$/BiOI-7 > $MoS_2$/BiOI-2 > BiOI > $MoS_2$. The results show that $MoS_2$ can efficiently improve the absorption of visible light and help the separation of electron-hole pairs; excessive $MoS_2$ will affect the ability of materials to absorb visible light, thus reducing the PEC of the materials.

Electrochemical impedance spectra (EIS) spectroscopy was used to evaluate the electron transfer kinetics (Figure 2b). The EIS was performed in 0.1 M PBS, which consisted of extruded semicircular portions and linear portions. Electron transfer resistance (Rct) can be quantified semicircle diameter. The values for the samples can be ranked

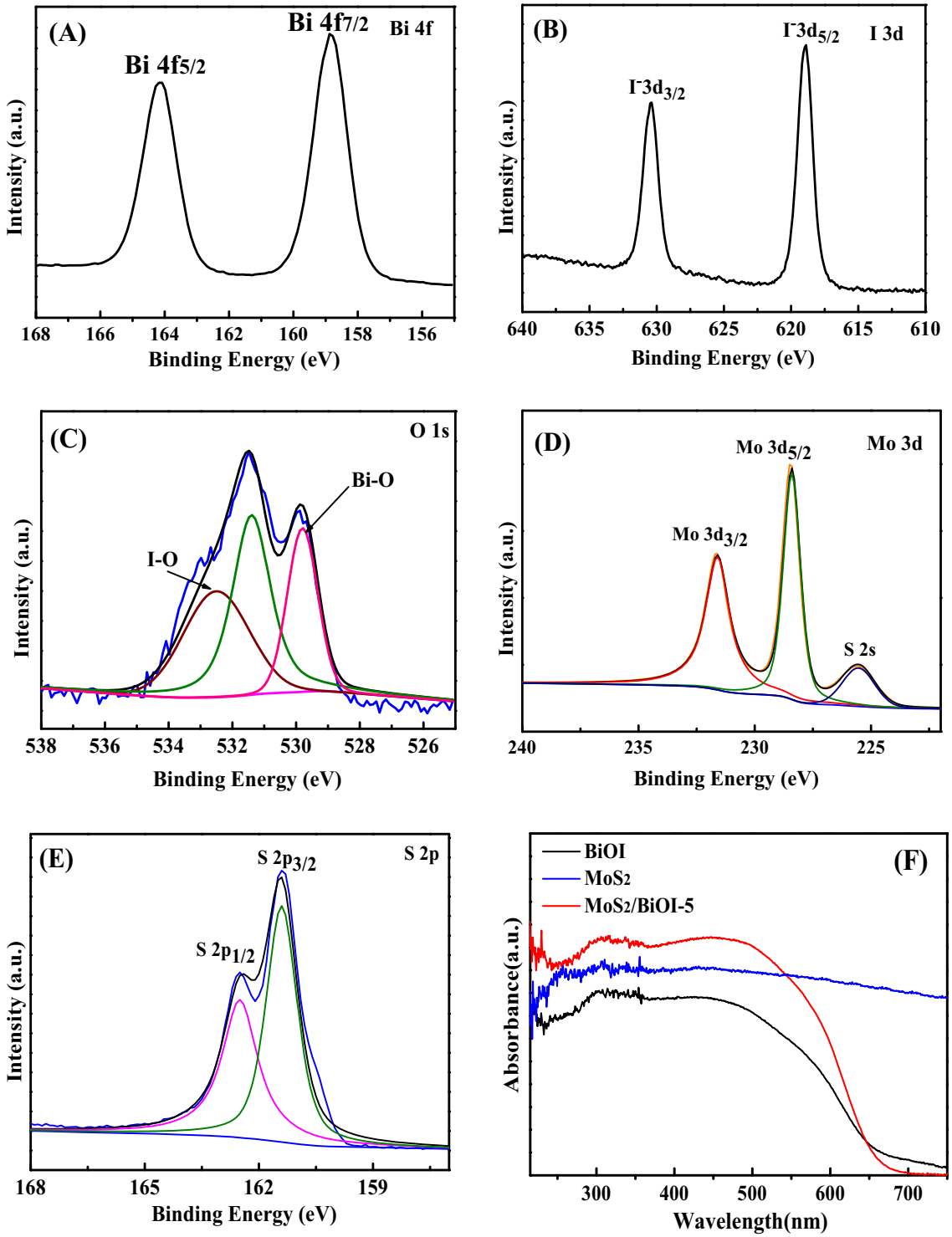


**Figure 4.** XPS spectrum of $MoS_2$/BiOI-5: (a) Bi 4f, (b) I 3d, (c) O 1s, (d) Mo 3d and (e) S 2p; UV–Vis diffuse reflectance spectra (f) of BiOI, $MoS_2$ and $MoS_2$/BiOI-5.

as: $MoS_2$ > BiOI > $MoS_2$/BiOI-2 > $MoS_2$/BiOI-7 > $MoS_2$/BiOI-5. The result indicates that $MoS_2$/BiOI-5 exist rapid electron transfer capability and good electrical conductivity. Based on the above results, $MoS_2$/BiOI-5 was selected to further investigate.

### 3.2 *Physical characterization*

The morphology of $MoS_2$, BiOI and $MoS_2$/BiOI-5 composites was characterized by SEM. Pure $MoS_2$ appears as curled and interlaced nanosheets in Figure 3a. Figure 3b clearly shows that BiOI consists

of a uniform sheet composed of a microsphere structure. The microstructure of $MoS_2$/BiOI-5 is shown in Figure 3c, d. It can be clearly observed that $MoS_2$/BiOI-5 is similar to BiOI. Figure 3e shows the HRTEM image of the box region in Figure 3d. High-resolution transmission electron microscopy (HRTEM) further confirmed the crystallinity and composition of the as-synthesized structure. The HRTEM (Figure 3e) examination displays three obvious lattice spacing of 0.62 nm and 0.301 nm, which are in close consistent with $MoS_2$ (002) and BiOI (102). In addition, the intimate contact between $MoS_2$ and BiOI may further confirm the formation of structure and favors charge separation and electron transfer.[6,25] Figure 2f–i respectively represents the distribution of Bi, I, Mo, and S element in $MoS_2$/BiOI-5. It is clear that all elements are evenly distributed throughout the $MoS_2$/BiOI-5, which show the synthesis was successfully prepared.

XPS was used to study the valence states of $MoS_2$/BiOI-5. The high resolution of Bi 4f, O1s, I 3d, Mo 3d and S 2p are shown in Figure 4a–e. As shown in Figure 4a, two main peaks of Bi 4f XPS spectra located at 158.8 eV and 164.2 eV. The peaks of 158.8 eV and 164.2 eV are assigned to Bi $4f_{7/2}$ and Bi $4f_{5/2}$ in standard $Bi^{3+}$.[31] The two peaks of $3d_{3/2}$ (630.2 eV) and $3d_{5/2}$ (618.5 eV) peaks of BiOI correspond to $I^{-1}$ (Figure 4b).[32] The O 1s peak is shown in the Figure 4c, the peak at 529.8 eV is attributed to the Bi–O bonds in BiOI, while the sharp signal peaks of 532.0 eV result from I–O bonds.[33] Mo $3d_{3/2}$ at 231.6 eV and Mo $3d_{5/2}$ at 228.4 eV are matched to $Mo^{4+}$ in Figure 4d.[34] In Figure 4e, S $2p_{1/2}$ at 162.5 eV and S $2p_{3/2}$ at 161.4 eV were attributed to $S^{2-}$.[35] All results show that the complex consists of $MoS_2$ and BiOI.

The absorption properties of BiOI and $MoS_2$/BiOI-5 were analyzed by UV–Vis DRS in Figure 4f. BiOI and $MoS_2$/BiOI-5 also could effectively utilize visible light has strong absorption capacity when the wavelength is less than 650 nm. Furthermore, $MoS_2$/BiOI-5 has obvious stronger absorption than BiOI in visible light ranges, which show that $MoS_2$ can improve the ability of BiOI to absorb visible light. Subsequently, photoluminescence spectra further studied the ability of prepared materials to separate electrons and holes. Figure 5 shows that $MoS_2$/BiOI-5 has the lowest intensity compared with BiOI, suggesting $MoS_2$/BiOI-5 has a low electron recombination rate.[36] According to the above discussion, $MoS_2$/BiOI-5 has excellent PEC performance.

The PEC mechanism of MoS2/BiOI is shown in Figure 6. Both BiOI and $MoS_2$ generate electron-hole pairs under visible light excitation, electrons are

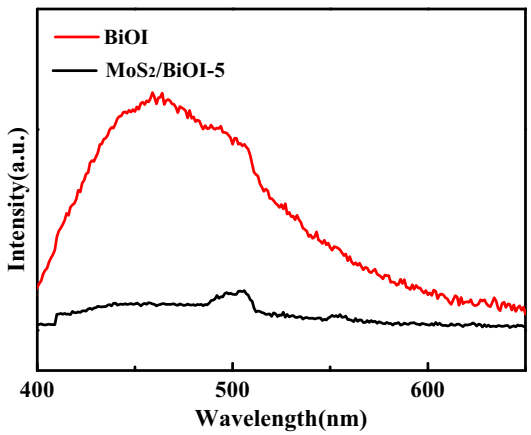


**Figure 5.** PL of the BiOI and $MoS_2$/BiOI-5 composites by 370 nm excitation wavelength.

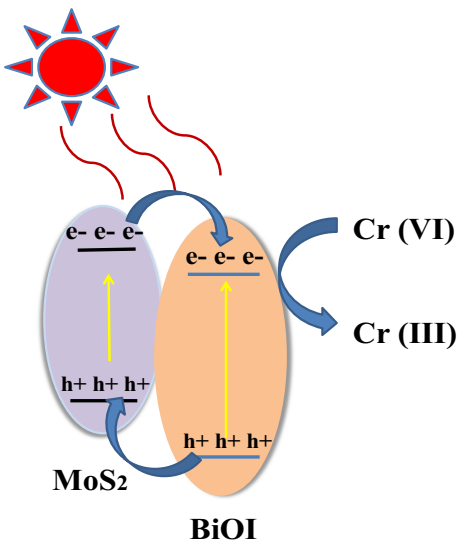


**Figure 6.** PEC mechanism of $MoS_2$/BiOI for the detection of Cr (VI).

excited to the conduction band (CB), and holes remain in the valence band (VB). At the same time, the excited electron transfer from CB ($MoS_2$) to the CB (BiOI) and the holes transfer from VB of BiOI to the VB of $MoS_2$ due to the dynamic principle,[37] which prevents the recombination of electrons and holes. Therefore, the adding of $MoS_2$ can effectively utilize the electron for reducing Cr (VI).

### 3.3 *Photoelectrochemical sensor*

Figure 7a shows the photocurrent performance of BiOI, $MoS_2$ and $MoS_2$/BiOI-5 at 0 V versus SCE under visible light excitation in 0.1 M PBS. The photocurrent response improved after Cr (VI) was added. At the same time, the photocurrent difference of $MoS_2$/BiOI-5 is higher than that of BiOI and $MoS_2$,

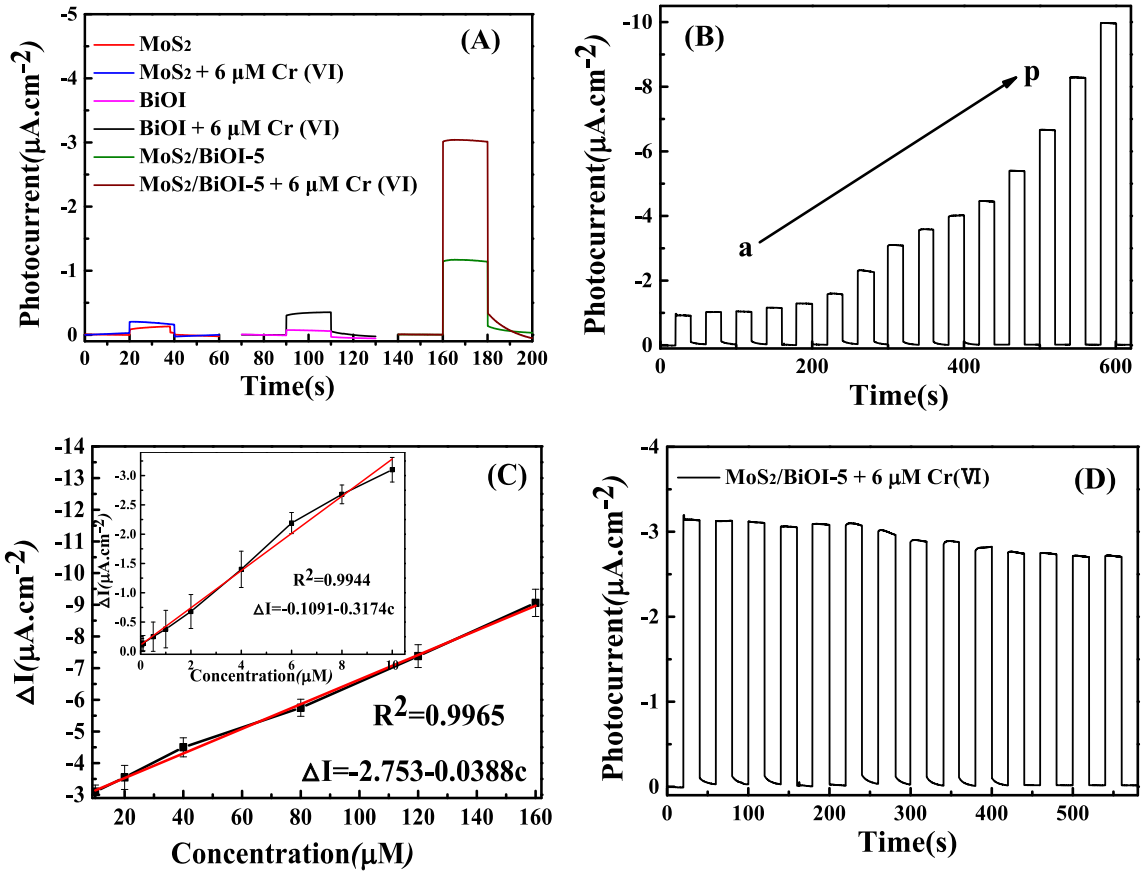


**Figure 7.** (a) Photocurrent responses of the $MoS_2$, BiOI and $MoS_2$/BiOI-5 in the absence and presence of 6 μM Cr (VI); (b) photocurrent responses of $MoS_2$/BiOI-5 toward Cr (VI) with increasing concentrations of Cr (VI); (c) the corresponding calibration plots of the Cr (VI) concentration; (d) stable photocurrent response curve of the $MoS_2$/BiOI-5 in the presence of 6 μM Cr (VI) in 0.1 M PBS at 0 V versus SCE with visible light excitation.

**Table 1.** Comparison of different methods for detecting Cr (VI).

| Method | Materials | Linear range (μM) | LOD | Refs. |
|---|---|---|---|---|
| Fluorescent | N, S-co-doped carbon dots | 1–40 | 0.52 μM | 38 |
| Colorimetric | GA-Au NPs | 2–20 | 2 μM | 39 |
| CV | Au | 5–100 | 2 μM | 40 |
| PEC | $Pb_5S_2I_6$ | 0.01–80 | 3 nM | 41 |
| PEC | Bi/BiOI | 1–230 | 0.3 μM | 6 |
| PEC | $MoS_2$/BiOI | 0.05–10<br>10–160 | 0.01 μM | This work |

which show that $MoS_2$ can efficiently improve the PEC performance for detecting Cr (VI).

In order to evaluate the PEC performance of the $MoS_2$/BiOI-5 for Cr (VI), the photocurrent change was measured at various concentrations of Cr (VI). Upon each addition of Cr (VI), the photocurrent response rises sharply in Figure 7b. The linear relationship between photocurrent and Cr (VI) concentration was obtained. Figure 7c shows two linear relationships of Cr (VI) based sensor of $MoS_2$/BiOI-5. From 0.05 to 10 μM, the linear regression equation is $\triangle I = 0.1091–0.3174c$ ($R^2 = 0.9944$). In the range of 10–160 μM, the linear relationship is $\triangle I = 2.753–0.0388c$ ($R^2 = 0.9965$). The detection limit of the sensor is 0.01 μM (S/N = 3). In addition, the comparison of $MoS_2$/BiOI-5 with other Cr (VI) sensors reported in the literature is shown in Table 1. Obviously, our sensor is superior to other Cr (VI) sensors in some aspects.

The stability of $MoS_2$/BiOI-5 was also checked by monitoring the photocurrent change by repeated light

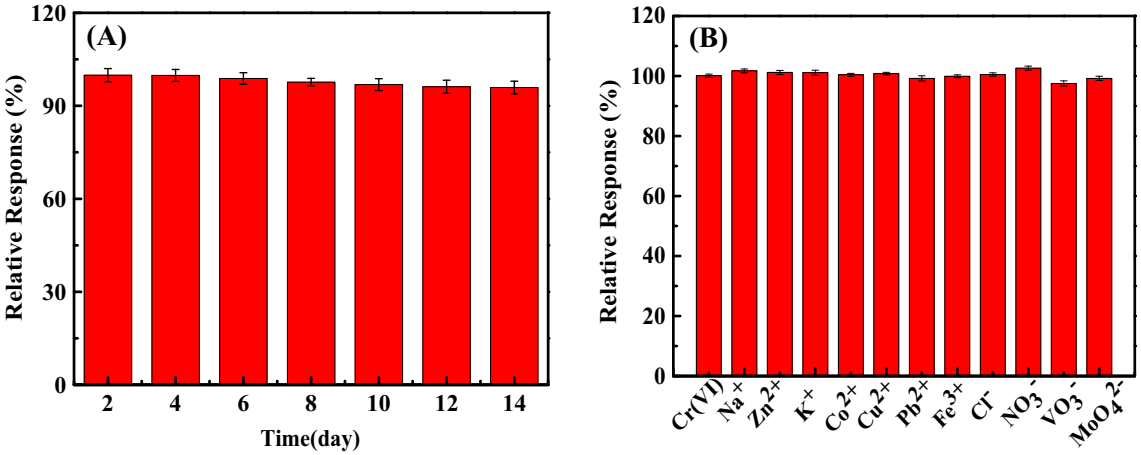


**Figure 8.** Stability tests of PEC sensor base on $MoS_2$/BiOI-5 towards Cr (VI); The photocurrent responses of 10 μM Cr(VI), 1000 μM of $Na^+$, $Zn^{2+}$, $K^+$, $Co^{2+}$, $Cu^{2+}$, $Pb^{2+}$, $Fe^{3+}$, $Cl^-$, $NO_3^-$, $VO_3^-$, $MoO_4^{2-}$ in 0.1 M PBS at 0 V versus SCE with visible light excitation.

**Table 2.** PEC detection of Cr (VI) in tap and lake water samples.

| | Cr (VI) concentration (μM) | | | | | |
|---|---|---|---|---|---|---|
| | Sample | Detected | Added | Found | Recovery (%) | RSD (%) |
| Tap | 1 | | 5.00 | 5.02 | 100.40 | 2.3 |
| | 2 | | 60.00 | 59.91 | 99.85 | 3.6 |
| | 3 | | 120.00 | 120.36 | 100.30 | 4.1 |
| Lake | 1 | Not found | 5.00 | 4.92 | 98.40 | 2.8 |
| | 2 | Not found | 60.00 | 60.26 | 100.43 | 4.3 |
| | 3 | Not found | 120.00 | 120.12 | 100.10 | 5.2 |

for 600 s (Figure 7d). Within 14 days, the photocurrent of $MoS_2$/BiOI-5 (Figure 8a) still remained 95.9% of its initial value. All results indicate that it had good stability. The photocurrent responses of $MoS_2$/BiOI-5 towards Cr (VI) and interfering substance were exhibited in Figure 8b, the photocurrent responses of interferences are negligible, suggesting $MoS_2$/BiOI-5 has an effective selectivity in the detection of Cr (VI).

In order to verify the actual reliability of the PEC sensor based on $MoS_2$/BiOI-5, the tap and lake water is taken as the real sample. The results are shown in Table 2. The relative standard deviation is less than 5.2%, and the recovery rate is 98.40–100.43%. These results show that the sensor based on $MoS_2$/BiOI-5 is reliable for Cr (VI) detection in actual samples.

## 4. Conclusions

In summary, in this work, we designed $MoS_2$/BiOI composites by using a two-step method. The layered $MoS_2$ modified BiOI was studied on the PEC detection of Cr (VI) under the visible light irradiation. $MoS_2$/BiOI shows the highest PEC efficiency of Cr (VI) compared with pure $MoS_2$ and BiOI, along with some other composites materials which have various contents of $MoS_2$. Subsequently, the sensor based on $MoS_2$/BiOI exhibits a wide linear range (0.05–160 μM), low detection limit (0.01 μM, S/N = 3) and excellent stability towards detecting Cr (VI). Moreover, the linear concentration range of 0.01 μM achieves the World Health Organization (WHO) specified the permissible limit of 0.96 μM. The study indicates that the sensor based on $MoS_2$/BiOI-5 has great application prospects for Cr (VI) PEC detection.

## Acknowledgements

This work was supported by the Natural Science Foundation of Liaoning Province (No. 20180540421).

## References

1. Tukur S A, Yusof N A and Hajian R 2015 Linear sweep anodic stripping voltammetry: determination of

chromium (VI) using synthesized gold nanoparticles modified screen-printed electrode *J. Chem. Sci.* **127** 1075
2. Malik S, Ghosh A and Sar P 2017 Employment of different spectroscopic tools for the investigation of chromium (VI) oxidation of acetaldehyde in aqueous micellar medium *J. Chem. Sci.* **129** 637
3. Chen G J, Han J C, Mu Y, Yu H M and Qin L P 2019 Two-stage chromium isotope fractionation during microbial Cr(VI) reduction *Water Res.* **148** 10
4. Gupta S, Yadav A and Verma N 2017 Simultaneous Cr (VI) reduction and bioelectricity generation using microbial fuel cell based on alumina-nickel nanoparticles-dispersed carbon nanofiber electrode *Chem. Eng. J.* **307** 729
5. Tu J W, Gan Y, Liang T, Wan H and Wang P 2018 A miniaturized electrochemical system for high sensitive determination of chromium (VI) by screen-printed carbon electrode with gold nanoparticles modification *Sens. Actuat. B-Chem.* **272** 582
6. Li M Y, Huang Y L, Wang S Q, Feng C Q, Wu H M and Mei H 2019 Visible light driven photoelectrochemical sensor for chromium (VI) BiOI microspheres decorated with metallic bismuth *Microchim. Acta* **186** 345
7. Ravishankar T N, Mauricio de O V, Ramakrishnappa T, Sergio R T and Dupont J 2017 Ionic liquid assisted hydrothermal syntheses of Au doped $TiO_2$ NPs for efficient visible-light photocatalytic hydrogen production from water, electrochemical detection and photochemical detoxification of hexavalent chromium ($Cr^{6+}$) *RSC Adv.* **7** 43233
8. Tang Y F, Chai Y, Liu X Q, Li L L, Yang L W, Liu P P, Zhou Y M, Ju H X and Cheng Y Z 2018 A photoelectrochemical aptasensor constructed with core-shell CuS-$TiO_2$ heterostructure for detection of microcystin-LR *Biosens. Bioelectron.* **117** 224
9. Dang X, Zhao H, Wang X, Sailijiang T, Chen S and Quan X 2018 Photoelectrochemical aptasensor for sulfadimethoxine using $gC_3N_4$ quantum dots modified with reduced graphene oxide *Microchim. Acta* **185** 345
10. Chen D Y, Jiang D, Du X J, Zhou L, Huang L Y, Qian J, Liu Q, Hao N, Li Y P and Wang K 2016 Engineering efficient charge transfer based on ultrathin graphite-like carbon nitride/$WO_3$ semiconductor nanoheterostructures for fabrication of high-performances non-enzymatic photoelectrochemical glucose sensor *Electrochim. Acta* **215** 305
11. Wang H, Ye H L, Zhang B H, Zhao F Q and Zeng B Z 2017 Electrostatic interaction mechanism based synthesis of a Z-scheme BiOI-CdS photocatalyst for selective and sensitive detection of $Cu^{2+}$ *J. Mater. Chem. A* **5** 10599
12. Ning S B, Lin H X, Tong Y C, Zhang X Y, Lin Q Y, Zhang Y Q, Long J L and Wang X X 2017 Dual couples Bi metal depositing and Ag@AgI islanding on BiOI 3D architectures for synergistic bactericidal mechanism of *E. coli* under visible light *Appl. Catal. B: Environ.* **204** 1
13. Tong H L, Jiang Y, Zhang Q, Jiang W C, Wang K L, Luo X X, Lin Z and Xia L X 2019 Boosting photoelectrochemical water oxidation with cobalt phosphide nanosheets on porous $BiVO_4$ *ACS Sustain. Chem. Eng.* **7** 769
14. Lv J L, Zhang J F, Liu J, Li Z, Dai K and Liang C H 2018 Bi SPR-promoted Z-scheme $Bi_2MoO_6$/CdS-diethylenetriamine composite with effectively enhanced visible light photocatalytic hydrogen evolution activity and stability *ACS Sustain. Chem. Eng.* **6** 696
15. Shi Y Q, Xiong X Y, Ding S P, Liu X F, Jiang Q Q and Hu J C 2018 In-situ topotactic synthesis and photocatalytic activity of plate-like BiOCl/2D networks $Bi_2S_3$ heterostructures *Appl. Catal. B Environ.* **220** 570
16. Chang C, Zhu L Y, Fu Y and Chu X L 2013 Highly active Bi/BiOI composite synthesized by one-step reaction and its capacity to degrade bisphenol A under simulated solar light irradiation *Chem. Eng. J.* **233** 305
17. Xu L, Li H N, Yan P C, Xia J X, Qiu, Xu Q, Zhang S Q, Li H M and Yuan S Q 2016 Graphitic carbon nitride/BiOCl composites for sensitive photoelectrochemical detection of ciprofloxacin *J. Colloid Interface Sci.* **483** 241
18. Sun X M, Lu J, Wu J, Guan D Y, Liu Q Z and Yan N Q 2019 Enhancing photocatalytic activity on gas-phase heavy metal oxidation with self-assembled BiOI/BiOCl microflowers *J. Colloid Interface Sci.* **546** 32
19. Wang K, Zhang W Z, Guan X Y, Liu Y X, Wei T and Guo W H 2018 Fabrication of PET/BiOI/SnO2 heterostructure nanocomposites for enhanced visible-light photocatalytic activity *Solid State Sci.* **82** 34
20. Zhang Y Q, Lin C, Lin Q, Jin Y B, Wang Y H, Zhang Z Z, Lin H X, Long J J and Wang X X 2018 CuI–BiOI/Cu film for enhanced photo-induced charge separation and visible light antibacterial activity *Appl. Catal. B Environ.* **235** 238
21. Zhu Y H, Liu X, Yan K and Zhang J D 2019 A cathodic photovoltammetric sensor for chloramphenicol based on BiOI and graphene nanocomposites *Sens. Actuat. B-Chem.* **284** 505
22. Yan P C, Jiang D S, Li H N, Cheng M, Xu L, Qian J C, Bao J, Xia J X and Li H M 2018 Exploitation of a photoelectrochemical sensing platform for catechol quantitative determination using BiPO4 nanocrystals/BiOI heterojunction *Anal. Chim. Acta* **1042** 11
23. Cai L, Yao J W, Li J B, Zhang Y F and Wei Y 2019 Sonochemical synthesis of BiOI–$TiO_2$ heterojunction with enhanced visible-light-driven photocatalytic activity *J. Alloy. Compd.* **783** 300
24. Huang H W, He Y, Du X, Chu P K and Zhang Y H 2015 A general and facile approach to heterostructured core/shell $BiVO_4$/BiOI p−n junction: room-temperature in situ assembly and highly boosted visible-light photocatalysis *ACS Sustain. Chem. Eng.* **3** 3262
25. Li Z Z, Meng X C and Zhang Z S 2018 Few-layer MoS2 nanosheets-deposited on Bi2MoO6 microspheres: a Zscheme visible-light photocatalyst with enhanced activity *Catal. Today* **315** 67
26. Trung T N, Seo D B, Quang N D, Kim D J and Kim E T 2018 Enhanced photoelectrochemical activity in the heterostructure of vertically aligned few-layer $MoS_2$ flakes on ZnO *Electrochim. Acta* **260** 150
27. Zhang J R, Zhao Y Q, Chen L, Yin S F and Cai M Q 2019 Density functional theory calculation on facet-dependent photocatalytic activity of $MoS_2$/CdS heterostructures *Appl. Surf. Sci.* **469** 27

28. Li H L, Yu K, Lei X, Guo B J, Fu H and Zhu Z Q 2015 Hydrothermal synthesis of novel $MoS_2/BiVO_4$ hetero-nanoflowers with enhanced photocatalytic activity and a mechanism investigation *J. Phys. Chem. C* **119** 22681
29. PesciOrcid F M, Sokolikova M S, Grotta C, Sherrell P C, Reale F, Sharda K, Ni N, Palczynski P and Mattevi C 2017 $MoS_2/WS_2$ Heterojunction for Photoelectrochemical Water Oxidation *ACS Catal.* **78** 4990
30. Liu X Q, Huo X H, Liu P P, Tang Y F, Xu J, Liu X H and Zhou Y M 2017 Assembly of $MoS_2$ nanosheet-$TiO_2$ nanorod heterostructure as sensor scaffold for photo-electrochemical biosensing *Electrochim. Acta* **242** 327
31. Zhang X, Wang X B, Wang L M, Wang W K, Long L L, Li W W and Yu H Q 2014 Synthesis of a highly efficient BiOCl single-crystal nanodisk photocatalyst with exposing {001} facets *ACS Appl. Mater. Interface* **6** 7766
32. Jiang J, Zhang X, Sun P B and Zhang L Z 2011 ZnO/BiOI heterostructures: photoinduced charge-transfer property and enhanced visible-light photocatalytic activity *J. Phys. Chem. C* **115** 20555
33. Xia J X, Di J, Li H T, Xu H, Li H M and Guo S J 2016 Ionic liquid-induced strategy for carbon quantum dots/BiOX (X = Br, Cl) hybrid nanosheets with superior visible light-driven photocatalysis *Appl. Catal. B Environ.* **18** 260
34. Shen J, Wu J, Pei L, Rodrigues M T F, Zhang Z, Zhang F, Zhang X, Ajayan P M and Ye M 2016 $CoNi_2S_4$-Graphene-2D-$MoSe_2$ as an advanced electrode material for supercapacitors *Adv. Energy Mater.* **6** 1600341
35. Zhang H C, Li Y J, Xu T H, Wang J B, Huo Z Y, Wan P B and Sun X M 2013 Amorphous Co-doped $MoS_2$ nanosheets coated on metallic $COS_2$ nanocubes as an excellent electrocatalyst for hydrogen evolution *J. Mater. Chem. A* **3** 15020
36. Wu R Y, Song H B, Luo N and Ji G J 2018 Hydrothermal preparation of 3D flower-like BiPO4/Bi2WO6 microsphere with enhanced visible-light photocatalytic activity *J. Colloid Interface Sci.* **524** 350
37. Bu Y Z, Xu J L, Li Y W, Liu Q and Zhang Z 2017 Enhanced photocatalytic activity of BiOI under visible light irradiation by the modification of $MoS_2$ *RSC Adv.* **7** 42398
38. Shen J, Shang S M, Chen X Y, Wang D and Cai Y 2017 Highly fluorescent N, S-co-doped carbon dots and their potential applications as antioxidants and sensitive probes for Cr (VI) detection *Sens. Actuat. B-Chem.* **248** 92
39. Dong C, Wu G H, Wang Z Q, Ren W Z, Zhang Y J, Shen Z Y, Li T H and Wu A Q 2015 Selective colorimetric detection of Cr (III) and Cr (VI) using gallic acid capped gold nanoparticles *Dalton Trans.* **45** 8347
40. Janik P, Zawisza B, Talik E and Sitko R 2018 Selective adsorption and determination of hexavalent chromium ions using graphene oxide modified with amino silanes *Microchim. Acta* **185** 117
41. Dashtian K, Ghaedi M and Shajati S 2019 Photo-Sensitive $Pb_5S_2I_6$ crystal incorporated polydopamine biointerface coated on nanoporous $TiO_2$ as an efficient signal-on photoelectrochemical bioassay for ultrasensitive detection of Cr (VI) ions *Biosens. Bioelectron.* **132** 105